

Hybrid Mask Generation for Infrared Small Target Detection with Single-Point Supervision

Wei jie He, Mushui Liu, Yunlong Yu*, Zheming Lu, Xi Li

Zhejiang University

Abstract

Single-frame infrared small target (IRST) detection poses a significant challenge due to the requirement to discern minute targets amidst complex infrared background clutter. Recently, deep learning approaches have shown promising results in this domain. However, these methods heavily rely on extensive manual annotations, which are particularly cumbersome and resource-intensive for infrared small targets owing to their minute sizes. To address this limitation, we introduce a Hybrid Mask Generation (HMG) approach that recovers high-quality masks for each target from only a single-point label for network training. Specifically, our HMG approach consists of a handcrafted Points-to-Mask Generation strategy coupled with a pseudo mask updating strategy to recover and refine pseudo masks from point labels. The Points-to-Mask Generation strategy divides two distinct stages: Points-to-Box conversion, where individual point labels are transformed into bounding boxes, and subsequently, Box-to-Mask prediction, where these bounding boxes are elaborated into precise masks. The mask updating strategy integrates the complementary strengths of handcrafted and deep-learning algorithms to iteratively refine the initial pseudo masks. Experimental results across three datasets demonstrate that our method outperforms the existing methods for infrared small target detection with single-point supervision.

Introduction

Infrared Small Target Detection (IRSTD), a critical task aimed at isolating minute objects from complex infrared backgrounds, holds immense potential for diverse applications spanning traffic management and public safety (Rawat, Verma, and Kumar 2020; Zhang and Tao 2021; Wu et al. 2022). However, in real-world scenarios, these targets often occupy a minute fraction of pixels and exhibit low signal intensities, rendering them highly susceptible to being obscured within the background imagery, posing significant challenges for accurate detection.

Recently, the deep-learning-based methods (Wang, Zhou, and Wang 2019; Zhang et al. 2022a; Yang et al. 2024; Zhang et al. 2024) have shown promising performances in pixel-level and instance-level metrics. However, the prevalent deep-learning approaches require a large amount of labeled data for model training, while annotating data at the

pixel level is arduous and time-consuming (Cheng, Parkhi, and Kirillov 2022; Li et al. 2021). Moreover, given the minute scale and poor separability of individual pixels, each pixel carries a heightened influence on the final results.

To mitigate these challenges, weakly-supervised models for image segmentation and detection (Bilen and Vedaldi 2016; Bearman et al. 2016; Wei et al. 2017), leveraging inexact annotations, have gained prominence as an efficient solution. The key to the weakly-supervised IRSTD paradigm is to obtain high-quality masks from the point-level annotations. LESPS (Ying et al. 2023) has tried to gradually expand point labels to mask labels through a label evolution mechanism. However, a notable performance disparity remains compared to fully-supervised performance. We attribute it primarily to the fact that the label evolution mechanism in LESPS, which is solely reliant on neural networks, is inherently implicit. Prior works (Li et al. 2023, 2024) have attempted to circumvent this limitation by developing masks through handcrafted algorithms, while often encountering difficulties in integrating high-level information that transcends the confines of the algorithmic framework. Furthermore, these methods rely on a centroid-based sampling strategy to acquire point labels, presupposing that the points cluster tightly around the centroids of targets. However, they inadequately address scenarios where the points deviate significantly from the centroids, leaving this aspect underexplored.

In this paper, we introduce a hybrid mask generation approach for IRSTD that enjoys the benefits of both handcrafted and deep-learning techniques. Specifically, our method consists of two stages to recover high-quality pseudo masks from the point labels. In the initial stage, based on the observation that the pixel differences within the target region and background region are smaller than the pixel differences between the target and background regions, we devise a handcrafted Point-to-Mask Generation strategy that adheres to a sequential process, progressing from point labels to bounding boxes, and subsequently to detailed initial pseudo masks. Then, initial pseudo masks are employed to supervise the training of the neural network, guiding its predictions to converge towards the masks. In the subsequent stage, we integrate both the predictions from the neural network and masks obtained from the handcrafted strategy to update pseudo masks. While the handcrafted strategy helps

*Corresponding Author.

correct the network’s predictions, the neural network integrates high-level information that might be overlooked by the handcrafted strategy in turn. This complementary nature enables us to obtain hybrid masks with enhanced quality. Moreover, we explore the benchmark of obtaining point labels with the uniform random sampling strategy and propose an iterative centroid rectification mechanism to mitigate the impact that random sampling point labels have on the quality of the pseudo masks.

To summarize, our key highlights are:

- We present a novel hybrid mask generation approach to leverage the complementary strengths of both deep-learning and handcrafted techniques to generate high-quality masks from single-point labels forIRSTD.
- We extend the sampling strategy of point labels from centroid-based to random sampling and propose an iterative centroid rectification mechanism to mitigate the performance gap arising from the variation in sampling strategy.
- Experimental results on three SIRST datasets demonstrate that the models trained with our hybrid masks set a new benchmark under single-point supervision.

Related Work

Infrared Small Target Detection.

In the early stage of infrared small target detection (IRSTD), the traditional paradigms (Deshpande et al. 1999; Chen et al. 2014; Gao et al. 2013) based on prior knowledge were often implemented through careful tuning of hyperparameters. However, in complex real-world scenarios, these methods lacked sufficient generalization capability. With the development of deep learning, the research focus has shifted from the traditional paradigm to the data-driven paradigm based on deep learning. For example, (Dai et al. 2021a) introduced an asymmetric contextual modulation module to effectively encode high-level contextual information while preserving finer details of targets. Meanwhile, (Li et al. 2022) presented a dense nested attention network to comprehensively exploit contextual cues of small targets. Furthermore, (Yuan et al. 2024) proposed a spatial-channel cross transformer network to reinforce the semantic differences between targets and clutter at multiple levels. Rather than focusing on designing advanced feature extraction or fusion modules, (Liu et al. 2024) introduced a novel scale and location sensitive loss function forIRSTD, which helps detectors better distinguish objects with varying scales and locations. Notably, (Chen et al. 2024) was the first to introduce heat conduction theories into theIRSTD network design, establishing a connection between the spatial and temporal information of pixel values during theIRSTD process. However, these methods are trained in a fully-supervised manner based on pixel-level annotated images, which incurs significant human annotation costs to obtain large-scale pixel-level labeled data for these data-driven models.

Weakly Supervised Segmentation with Points.

(Bearman et al. 2016) was the first work to directly employ single-point supervision in the network training pro-

cess, and demonstrated that under a limited annotation budget, models trained with point supervision outperform those trained with pixel-level supervision. (Laradji et al. 2020) constructed a network with two branches to predict the location of the target and group pixels with similar embeddings, in order to obtain the segmentation mask for the identified target. Under the condition of multi-point supervision, (Qian et al. 2019) achieved semantic scene parsing by optimizing the intra- and inter-category embedding feature consistency among the annotated points. Additionally, some works have extended single-point supervision to the domain ofIRSTD. For instance, (Ying et al. 2023) discovered the phenomenon of mapping degradation during deep neural network training, and proposed a label evolution framework that gradually expands the initial point-level labels to provide better supervision quality. Similarly, (Li et al. 2023) utilized a Monte Carlo linear clustering method to predict high-quality pseudo masks from point labels for training supervision. Additionally, (Li et al. 2024) designed a dedicated energy functional based on the intensity expectation difference between the areas around the target, realizing the prediction of pseudo masks from point labels. The existing methods typically use a centroid-based sampling strategy to obtain the point labels while the scenario where the points deviate from the centroids lacks exploration. In this paper, we explore the weakly supervised point-level annotation benchmark that randomly and uniformly samples a single point from the target region as the point label.

Method

The proposed approach comprises two stages. First, initial pseudo masks are recovered from the point labels of the training samples, which are then leveraged to train anIRSTD model. Subsequently, the initial pseudo masks and the model’s predictions were integrated to form hybrid masks for the retraining of the model.

Points-to-Mask Generation

Given an infrared image and its point label, the initial pseudo mask is obtained with the following two steps, as illustrated in Fig. 1. The first step, Points-to-Box, involves utilizing the provided point label to predict a bounding box that encapsulates the target. Subsequently, in the Box-to-Mask step, the probability of each pixel in the bounding box belonging to the target is predicted in a direction-specific manner to derive the final pseudo masks.

Points-to-Box. We propose to predict a bounding box that encapsulates the target leveraging the observation that the pixel differences within the target and background regions are significantly smaller than inter-region differences. This involves first identifying the target, the transition, and the background regions based on the pixel differences around the point label. Then, we determine a threshold using the pixels located at the intersection of the background and transition regions to locate the boundary between the target and pure surroundings in each direction. Finally, we obtain the bounding box by combining the boundary predictions in four directions.

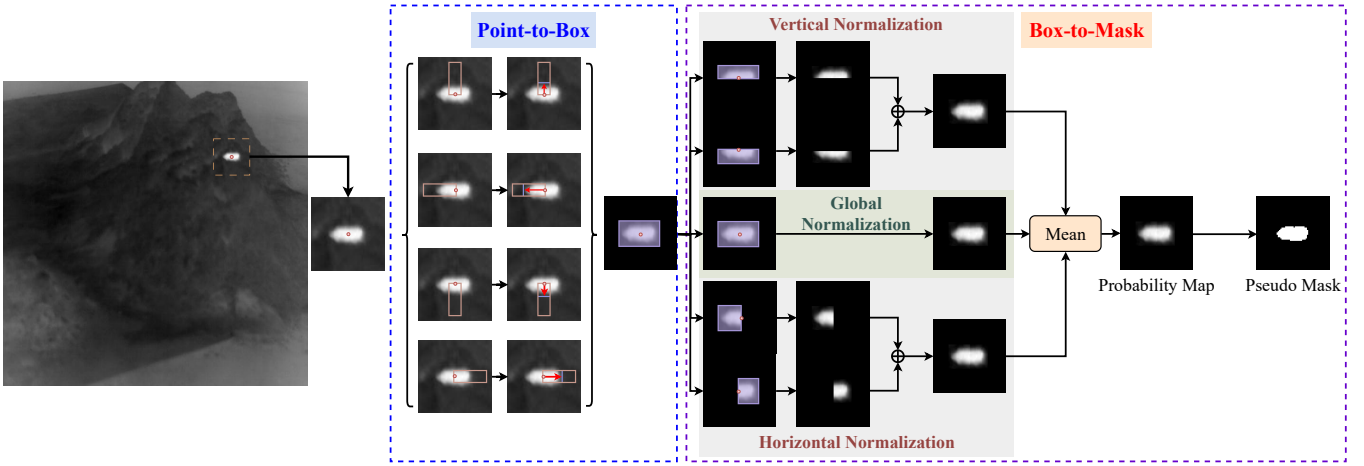


Figure 1: The flowchart outlining the process of deriving the pseudo mask from a point label of the target.

We take the determination of the left boundary as an example to elucidate the process of bounding box prediction. First, we obtain a rectangular area of interest in the infrared image by taking the point label as the reference point u_0 and expanding it L_{ep} pixels to the left, L_{dp} pixels in upward and downward directions, as shown in Fig. 2(a). For this rectangular area, we obtain vertical maximum vector and vertical average vector by separately finding the maximum and average pixel values along the vertical dimension, respectively, as shown in Fig. 2(b). Then we calculate the absolute differences between adjacent elements in vertical maximum vector as the pixel differences D along the prediction direction in Fig. 2(c-d). As observed from Fig. 2(d), while the overall pixel differences are small, they exhibit a distribution with the middle region being relatively larger compared to the two ends. We calculate the mean of D as the difference threshold and divide the area into three regions: the target, transition, and background regions. After obtaining the position of the boundary where the transition region meets the background region, the corresponding value in the vertical average vector is designated as the background threshold. Starting from the rightmost value in the vertical average vector, we search leftward until a position is reached where the value crosses the background threshold, and that position is identified as the left boundary, as shown in Fig. 2(e-f).

Similarly, we predict the remaining right, upward, and downward boundaries, thereby determining the bounding box that encompasses the target.

Box-to-Mask. After obtaining the bounding box, we proceed to evaluate the pixels within it. Specifically, we establish a pixel threshold σ to distinguish the background and the target. In addition to incorporating the mean pixel value within the bounding box, we also include the pixel value at the position of u_0 in the calculation of σ , to obtain more accurate predictions and mitigate the propagated impact of the potential bounding box prediction errors. That is:

$$\sigma = \alpha * I(u_0) + (1 - \alpha) * \frac{1}{N} \sum_{u \in U} I(u) \quad (1)$$

where $I(u)$ denotes the pixel value at the spatial location u in the infrared image. The set U encompasses all pixels contained within the bounding box and N is the number of elements in U .

The pixels with values higher than σ are more likely to belong to the target, while others are more likely to belong to the background. We then normalize the pixel values to obtain the target probabilities within U by uniformly distributing pixel values lower than σ into a target probability $P(u)$ range of 0-0.5, and similarly, distributing pixel values higher than σ into a target probability $P(u)$ range of 0.5-1. That is:

$$P(x, y) = \begin{cases} \frac{I(u) - Min}{\sigma - Min} * 0.5 & I(u) \leq \sigma \\ 1 - \frac{Max - I(u)}{Max - \sigma} * 0.5 & I(u) > \sigma \end{cases} \quad (2)$$

where Min and Max are the minimum and maximum pixel value within U .

Considering the distinct characteristics of target and background pixels in different directions, we go beyond the global analysis to get the global probability map P_g within U and perform direction-specific probability predictions. Specifically, U is divided into separate subregions along four cardinal directions (upwards, downwards, leftwards, and rightwards) from u_0 and each subregion is normalized to a probability map. In this way, the probability maps for the upwards and downwards directions are concatenated to achieve vertical bidirectional normalization obtaining P_v , while those for the leftwards and rightwards directions are concatenated to achieve horizontal bidirectional normalization obtaining P_h . The final target probability map P_f is derived by averaging the probabilities across three distinct probability maps. Following this aggregation, a threshold of 0.5 is applied to P_f , converting it into a binary pseudo mask PM . That is:

$$P_f(u) = \frac{P_g(u) + P_v(u) + P_h(u)}{3}, \quad (3)$$

$$PM(u) = \begin{cases} 1 & P_f(u) \geq 0.5 \\ 0 & P_f(u) < 0.5 \end{cases} \quad (4)$$

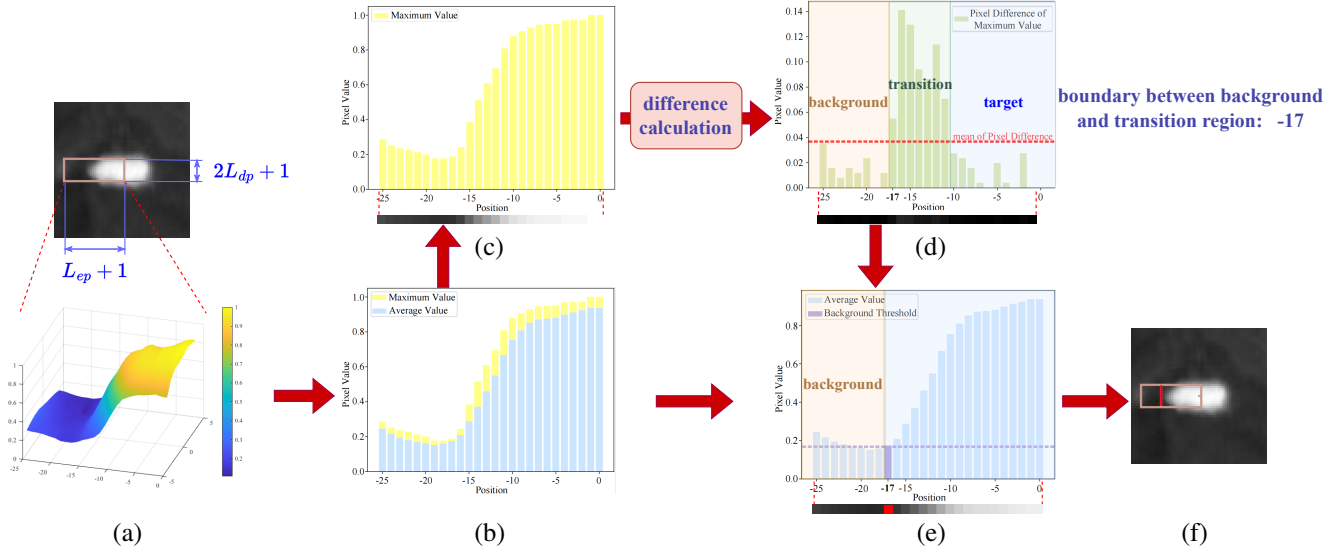


Figure 2: The flowchart of obtaining the left boundary of the bounding box from the point label.

After obtaining the initial pseudo masks for the training samples, these samples with masks can subsequently be employed to train neural networks.

Pseudo Mask Updating

After training the network with initial pseudo masks, the predictions of the neural network contain implicit information that is difficult for handcrafted methods to capture. The pseudo masks from handcrafted methods can also provide reliable assistance in correcting the neural network’s predictions. Therefore, to achieve complementarity between handcrafted methods and neural network capabilities, we comprehensively utilize the point label, initial pseudo mask, and the prediction probability map of the neural network to update the pseudo mask. As depicted in Fig. 3, the updating process encompasses two key modules: a missed detection retrieving module and a false alarm filtering module, to achieve the correction of the neural network’s predictions.

Missed Detection Retrieving. To address the issue of missed detections in neural network predictions, we take the external rectangles of each connected component in initial pseudo masks to simulate the previously obtained bounding boxes. We determine whether a target is detected by the neural network by checking if the maximum predicted probability within the bounding box exceeds the detection threshold of 0.5. If so, we consider the target at that location is successfully detected; otherwise, we identify the target within the region as in missed detection status. For the targets in missed detection status, we reset the detection threshold to the mean predicted probability within the bounding box. Then we perform early binarization in the region with the new threshold. By picking out pixels with relatively higher predicted probabilities, we ensure that at least one target is detected within the region, thereby mitigating the issue of missed detection. Subsequently, the entire prediction probability map is binarized to obtain the prediction mask with a detection thresh-

old of 0.5.

False Alarm Filtering. To mitigate the false alarm issue in neural network predictions, we calculate the centroids of each connected component within the prediction mask and compare them with the point labels. We consider a connected component in prediction mask as in false alarm status whose centroid’s L_1 distance to any point from point label is greater than a certain value δ . After filtering out all connected components in false alarm status, we complete the correction of the neural network’s prediction mask.

Union Combination. Finally, the corrected prediction mask P from the neural network will be fused with the pseudo mask from handcrafted methods to combine the advantages of both. When the sampling strategy for the point labels is centroid-based, we directly combine P with the initial pseudo mask I through a union operation to get the hybrid pseudo mask. Otherwise, when the sampling strategy is changed to random sampling, to reduce the performance gap arising from changing, we utilize the centroids of the connected components in P to simulate the target centroids in the ground truth mask, thereby obtaining points more reliable than the initial points in point label. We then apply the Points-to-Mask Generation (PMG) to predict these new points, obtaining calibrated mask C . By taking the intersection of C and I , we obtain a handcrafted mask with higher confidence, which is then combined with P through a union operation to get the final hybrid pseudo mask.

Centroid Rectification Mechanism.

When the sampling strategy of point label is not centroid-based, i.e., random sampling, the quality of the pseudo masks experiences a significant decline. To mitigate this issue, we design a centroid rectification mechanism Alg. 1 that iteratively adjusts the point labels to gradually move towards target centroids.

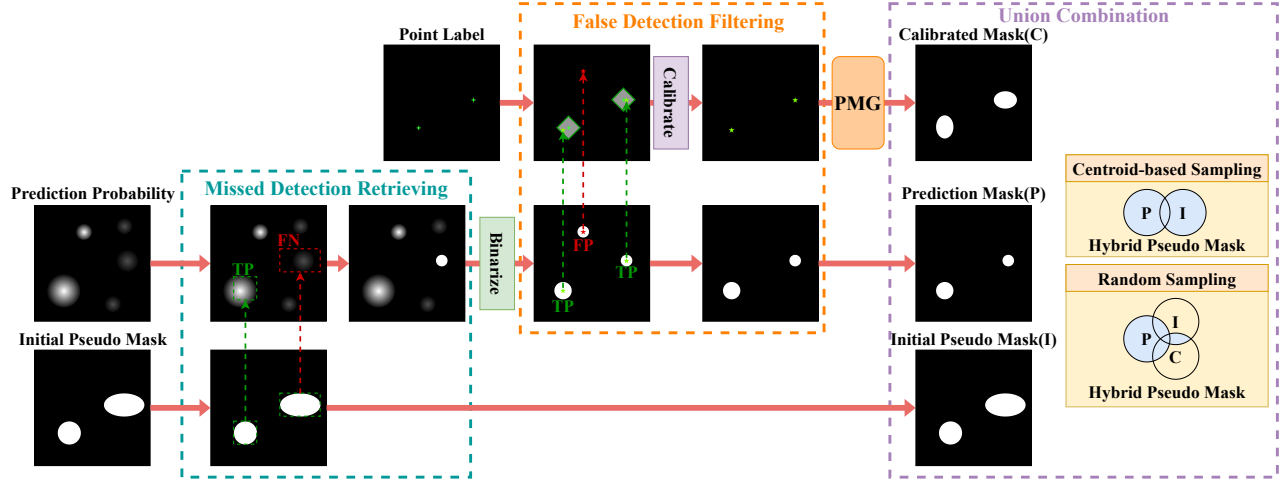


Figure 3: The flowchart of updating the pseudo mask from the prediction probability, the initial mask, and the point label.

Algorithm 1: Centroid Rectification Mechanism

Input: infrared image IR , initial points IP

Output: pseudo mask M

- 1: Let $R \leftarrow \emptyset, O \leftarrow IP$
 - 2: **while** $O \not\subseteq R$ **do**
 - 3: $R \leftarrow R \cup O$
 - 4: $M \leftarrow \text{Points_to_Mask}(IR, O)$
 - 5: $O \leftarrow \text{Centroids_Calculation}(M)$
 - 6: **end while**
 - 7: **return** M
-

In the initial phase, the initial points from the point labels are assigned to the set O , and an empty set R is initialized to record the points encountered during the iteration process. The core of the iterative loop is structured as follows: The elements in O will be added in R , and used to generate a pseudo mask. Then the centroids of each connected component will be calculated from the generated pseudo masks and used to replace elements in O . The core will iteratively cycle until the condition that O is a subset of R is satisfied. The pseudo masks generated in the last iteration are output as the results.

Experiments

Datasets and Implementation Details

We conduct evaluations on three popular datasets: NUAA-SIRST (Dai et al. 2021b), IRSTD-1K (Zhang et al. 2022b) and NUDT-SIRST (Li et al. 2022) and follow the same splits and data augmentation as (Ying et al. 2023) to partition three datasets into their respective training and test sets and process images during training. L_{ep} was set to 10 for NUDT-SIRST and 25 for the remaining datasets. L_{dp} , α and δ were set to 4, 0.15 and 30 for all datasets, respectively. The networks were trained with Soft-IoU loss function and optimized using the Adam (Kingma and Ba 2015) method, with a batch size of 8. The initial learning rate was set to 1e-3 and

was reduced with CosineAnnealingLR scheduler. The training epochs of the two stages were set to 250 and 1500, respectively. Without specification, default SIRST model used in experiments is DNANet (Li et al. 2022). All models were implemented in PyTorch (Paszke et al. 2019) on a PC with an Nvidia GeForce 3090 GPU. In the experiment, two pixel-level metrics (i.e., Intersection over Union (IoU), and the False alarm rate (F_a)) and one instance-level metric (the Probability of detection (P_d)) are employed for performance evaluation.

Comparison with State-of-the-Art Competitors

Two classic SIRST methods, namely ACM (Dai et al. 2021a) and DNA-Net (Li et al. 2022), serve as the training models in our study. For comparison, we select two weakly-supervised competitors, both of which utilize centroid point labels. From the results shown in Table 1, we observe that our method performs very competitively on all three datasets. Specifically, when employing the centroids of the targets as the point labels, our method significantly outperforms the rivals (Ying et al. 2023) and (Li et al. 2023) and performs close to the counterpart with full supervision in terms of both IoU and P_d metrics on ACM. Furthermore, when utilizing random points within the targets as the point labels, our method even outperforms the competitors that rely on the centroids. When deployed on the advanced training model DNANet (Li et al. 2022), our method maintains its superiority on average across all three datasets, as evidenced by its consistently high performance.

Comparison of Initial Pseudo Mask

From the results in Table 2, we observe that our initial pseudo masks achieves slightly lower performance than the competitor MCLC (Li et al. 2023) on IRSTD-1K and NUAA-SIRST datasets, but significantly improves performance on NUDT-SIRST dataset. We speculate that the reason is that compared with the other two datasets, the pixel difference between the target and background regions in

Methods	Supervision	NUAA-SIRST			IRSTD-1K			NUDT-SIRST			Mean		
		IoU \uparrow	P _d \uparrow	F _a \downarrow	IoU \uparrow	P _d \uparrow	F _a \downarrow	IoU \uparrow	P _d \uparrow	F _a \downarrow	IoU \uparrow	P _d \uparrow	F _a \downarrow
ACM	Fully (Dai et al. 2021a)	70.33	93.91	3.73	60.97	90.58	21.78	67.08	95.97	10.18	66.13	93.49	11.90
	Weakly (Centroid) (Ying et al. 2023)	49.23	89.35	40.95	41.44	88.89	60.46	42.09	91.11	38.24	44.25	89.78	46.55
	Weakly (Centroid) (Li et al. 2023)	67.08	92.01	19.80	56.53	82.31	25.05	57.74	92.38	16.77	60.45	88.90	20.54
	Weakly (Centroid) (Ours)	70.02	92.02	28.13	59.21	94.28	71.81	60.58	92.06	42.54	63.27	92.79	47.49
	Weakly (Random) (Ours)	67.90	93.54	12.90	58.32	94.28	51.66	59.47	88.99	40.38	61.90	92.27	34.98
DNANet	Fully (Li et al. 2022)	76.24	97.71	12.80	68.44	94.77	8.81	86.36	97.39	6.90	77.01	96.62	9.50
	Weakly (Centroid) (Ying et al. 2023)	61.95	92.02	18.17	52.09	88.88	16.09	57.99	94.71	26.45	57.34	91.87	20.24
	Weakly (Centroid) (Li et al. 2023)	72.86	96.95	14.43	62.23	92.13	24.14	70.52	95.55	33.20	68.54	94.88	23.92
	Weakly (Centroid) (Ours)	72.85	95.06	13.31	61.58	93.94	18.16	73.78	96.72	23.35	69.40	95.24	18.27
	Weakly (Random) (Ours)	72.76	95.82	11.46	61.68	92.59	15.68	71.90	94.92	38.10	68.78	94.44	21.75

Table 1: IoU ($\times 10^2$), P_d ($\times 10^2$) and F_a ($\times 10^6$) values of different methods achieved on NUAA-SIRST (Dai et al. 2021b), IIRSTD-1K (Zhang et al. 2022b) and NUDT-SIRST (Li et al. 2022) datasets. “Fully”, “Centroid”, and “Random” represent methods under full supervision, centroid, and random point supervision.

Method	IRSTD-1k	NUAA-SIRST	NUDT-SIRST	Mean
MCLC (Li et al. 2023)	68.80	76.30	60.20	68.43
Ours	65.79	74.22	70.98	70.33

Table 2: IoU (%) of pseudo mask prediction on three datasets in the training stage.

Sampling	Method	IRSTD-1K	NUAA-SIRST	NUDT-SIRST	Mean
Centroid	Initial	65.79	74.22	70.98	70.33
	Prediction	66.03	73.71	73.81	71.18
	Hybrid	69.56	76.29	74.36	73.40
Random	Initial	60.04	72.80	58.69	63.84
	Calibrated	64.40	73.48	67.13	68.34
	Prediction	64.15	72.90	71.13	69.39
	Hybrid	67.37	75.58	70.77	71.24

Table 3: IoU (%) impacts of pseudo mask updating on three datasets.

NUDT-SIRST dataset is relatively small, posing significant challenges for small target detection. Our method, by its capability to discern small targets based on the relative magnitude of pixel difference, demonstrates remarkable adaptability in selecting optimal prediction strategies tailored to the unique pixel distributions of targets and backgrounds, thereby contributing to its superior performance on NUDT-SIRST dataset.

Impacts of Updating Strategy

Table 3 represents the impacts of the pseudo mask updating. From the results, we observe that the model trained with the initial pseudo masks performs better than the initial supervision, especially on random sampling strategy. Additionally, we observed that the calibrated masks have better quality compared to the initial pseudo masks on random sampling strategy, verifying that the points derived from the corrected prediction masks are more reliable than the initial points. Besides, when applying the pseudo mask updating strategy, the quality of hybrid pseudo masks is further improved.

Method	MDR	FAF	IRSTD-1K	NUAA-SIRST	NUDT-SIRST	Mean
Centroid	\times	\times	62.99	73.38	73.17	69.85
	\checkmark	\times	63.01	73.52	73.17	69.90
	\checkmark	\checkmark	66.02	73.57	73.80	71.13
	\checkmark	\checkmark	66.03	73.71	73.81	71.18
Random	\times	\times	60.73	71.81	70.45	67.66
	\checkmark	\times	60.88	72.37	70.46	67.90
	\times	\checkmark	64.01	72.33	71.11	69.15
	\checkmark	\checkmark	64.15	72.90	71.13	69.39

Table 4: Ablation results in terms of IoU (%) of Missed Detection Retrieving (MDR) and False Alarm Filtering (FAF) on three datasets during the pseudo mask updating.

Method	IRSTD-1k	NUAA-SIRST	NUDT-SIRST	Mean
Centroid	65.79	74.22	70.98	70.33
Random	52.07	67.82	54.29	58.06
Random + Rectification	60.04	72.80	58.69	63.84

Table 5: IoU (%) impacts of centroid rectification mechanism when using random points as the initial annotations on the three datasets.

Impacts of Updating Correction Module

Table 4 shows the ablation study of both Missed Detection Retrieving and False Alarm Filtering during the pseudo mask updating stage under both centroid-based and random sampling strategies. From the results, we observe that both Missed Detection Retrieving and False Alarm Filtering could improve the quality of the mask prediction. The improvement brought by Missed Detection Retrieving is relatively modest, while the improvement from False Alarm Filtering is more pronounced. Note that the improvement under random sampling strategy is more significant than that under centroid-based sampling strategy. This suggests that when the initial sampling is more random and less representative of the true distribution, the application of correction methods yields greater benefits in refining the prediction results.

Impacts of Centroid Rectification Mechanism

In this experiment, we evaluate the impacts of centroid rectification mechanism on random sampling strategy. As shown in Table 5, when the sampling strategy is changed to random

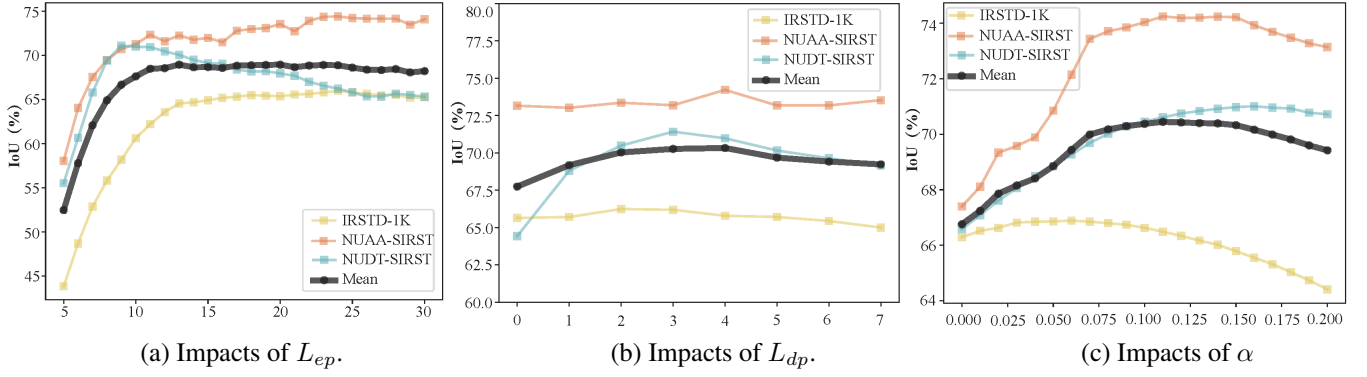


Figure 4: Ablation study of Points-to-Box during Points-to-Mask Generation process in terms of L_{ep} , L_{dp} , and α .

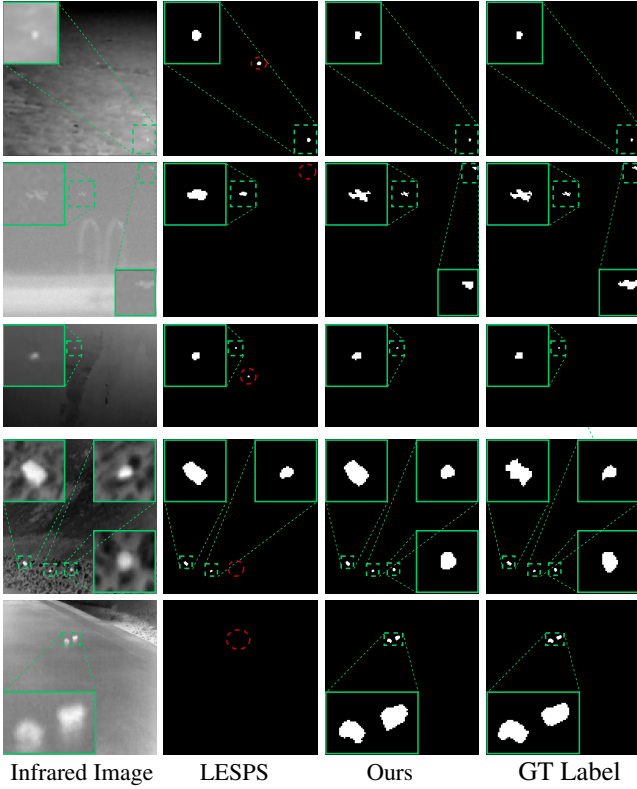


Figure 5: Some qualitative results on three datasets. For better visualization, the target area is enlarged and targets in missed detection or false alarm status are delineated in red.

sampling, the overall IoU of pseudo masks drops by approximately 12%. This demonstrates that the distribution of sampling points within the target significantly impacts the quality of our pseudo mask generation. When applying the rectification mechanism, the performances of all three datasets increase significantly. Consequently, we conclude that when the constraints on the initial sampling points are weak or relatively random, the rectification mechanism can effectively compensate for the decline in pseudo masks' quality.

Ablation Study During Initial Mask Generation

Fig. 4 illustrates the impact of hyperparameters L_{ep} , L_{dp} , and α during Points-to-Mask Generation process on three datasets. As depicted in Fig. 4(a), as L_{ep} increases, there is a rapid improvement in the quality of the generated pseudo masks. However, as L_{ep} continues to increase beyond a certain point, the pseudo masks' quality gradually declines. This phenomenon arises because sufficient L_{ep} is necessary to encompass the transition region and reach the background region while excessive L_{ep} can easily encounter transitions between different backgrounds in the background region and mislead the prediction of the target boundary. Fig. 4(b) showcases the influence of L_{dp} on pseudo masks' quality. The results indicate that some extension perpendicular to prediction direction aids boundary estimation for the reason that providing a more comprehensive target representation is necessary to effectively locate the target boundaries, when facing irregularly-shaped targets. Lastly, Fig. 4(c) explores the effect of α on pseudo masks' quality. It reveals that considering sampling point's value in pixel threshold enhances the accuracy of pseudo mask generation.

Qualitative Results

Fig. 5 shows the qualitative results of network's prediction on three datasets. Compared with LESPS (Ying et al. 2023), the network trained with the pseudo mask generated by our method achieves better instance-level and pixel-level detection, with lower false alarm and missed detection and more precise details. This superior performance can be attributed to the high-quality supervision provided by our hybrid masks.

Conclusion

In this paper, we have proposed a Hybrid Mask Generation approach (HMG) to obtain high-quality pseudo masks from point labels by combining both strengths of deep-learning and handcrafted strategies. Specifically, we design a handcrafted Point-to-Mask Generation method which shows robust adaptability across diverse scenarios to recover initial pseudo masks from point labels and a pseudo mask updating method that enables the integration of deep-learning and handcrafted strategies. Moreover, we extend the sampling

strategy of point labels from centroid-based to random sampling and propose an iterative centroid calibration mechanism to mitigate the performance gap arising from the variation in sampling strategy. Experimental results on three SIRST datasets demonstrated that our method overall outperforms other existing method for infrared small target detection with single-point supervision.

References

- Bearman, A.; Russakovsky, O.; Ferrari, V.; and Fei-Fei, L. 2016. What's the point: Semantic segmentation with point supervision. In *European Conference on Computer Vision*, 549–565.
- Bilen, H.; and Vedaldi, A. 2016. Weakly supervised deep detection networks. In *Proceedings of the IEEE/CVF Conference on Computer Vision and Pattern Recognition*, 2846–2854.
- Chen, C. L. P.; Li, H.; Wei, Y.; Xia, T.; and Tang, Y. Y. 2014. A Local Contrast Method for Small Infrared Target Detection. *IEEE Transactions on Geoscience and Remote Sensing*, 52(1): 574–581.
- Chen, T.; Tan, Z.; Chu, Q.; Wu, Y.; Liu, B.; and Yu, N. 2024. TCI-Former: Thermal Conduction-Inspired Transformer for Infrared Small Target Detection. In *Proceedings of the AAAI Conference on Artificial Intelligence*.
- Cheng, B.; Parkhi, O.; and Kirillov, A. 2022. Pointly-Supervised Instance Segmentation. In *Proceedings of the IEEE/CVF International Conference on Computer Vision*, 2607–2616.
- Dai, Y.; Wu, Y.; Zhou, F.; and Barnard, K. 2021a. Asymmetric Contextual Modulation for Infrared Small Target Detection. In *IEEE Winter Conference on Applications of Computer Vision*, 949–958.
- Dai, Y.; Wu, Y.; Zhou, F.; and Barnard, K. 2021b. Attentional local contrast networks for infrared small target detection. *IEEE Transactions on Geoscience and Remote Sensing*, 59(11): 9813–9824.
- Deshpande, S. D.; Er, M. H.; Venkateswarlu, R.; and Chan, P. 1999. Max-mean and max-median filters for detection of small targets. In *Optics & Photonics*.
- Gao, C.; Meng, D.; Yang, Y.; Wang, Y.; Zhou, X.; and Hauptmann, A. G. 2013. Infrared Patch-Image Model for Small Target Detection in a Single Image. *IEEE Transactions on Image Processing*, 22(12): 4996–5009.
- Kingma, D. P.; and Ba, J. 2015. Adam: A Method for Stochastic Optimization. In *International Conference on Learning Representations*.
- Laradji, I. H.; Rostamzadeh, N.; Pinheiro, P. O.; Vazquez, D.; and Schmidt, M. 2020. Proposal-based instance segmentation with point supervision. In *IEEE International Conference on Image Processing*, 2126–2130.
- Li, B.; Wang, Y.; Wang, L.; Zhang, F.; Liu, T.; Lin, Z.; An, W.; and Guo, Y. 2023. Monte Carlo linear clustering with single-point supervision is enough for infrared small target detection. In *Proceedings of the IEEE/CVF International Conference on Computer Vision*, 1009–1019.
- Li, B.; Xiao, C.; Wang, L.; Wang, Y.; Lin, Z.; Li, M.; An, W.; and Guo, Y. 2022. Dense nested attention network for infrared small target detection. *IEEE Transactions on Image Processing*, 32: 1745–1758.
- Li, H.; Yang, J.; Xu, Y.; and Wang, R. 2024. A Level Set Annotation Framework With Single-Point Supervision for Infrared Small Target Detection. *IEEE Signal Processing Letters*, 31: 451–455.
- Li, Y.; Zhao, H.; Qi, X.; Wang, L.; Li, Z.; Sun, J.; and Jia, J. 2021. Fully Convolutional Networks for Panoptic Segmentation. In *Proceedings of the IEEE/CVF Conference on Computer Vision and Pattern Recognition*, 214–223.
- Liu, Q.; Liu, R.; Zheng, B.; Wang, H.; and Fu, Y. 2024. Infrared Small Target Detection with Scale and Location Sensitivity. In *Proceedings of the IEEE/CVF Conference on Computer Vision and Pattern Recognition*, 17490–17499.
- Paszke, A.; Gross, S.; Massa, F.; Lerer, A.; Bradbury, J.; Chanan, G.; Killeen, T.; Lin, Z.; Gimelshein, N.; Antiga, L.; Desmaison, A.; Köpf, A.; Yang, E. Z.; DeVito, Z.; Raison, M.; Tejani, A.; Chilamkurthy, S.; Steiner, B.; Fang, L.; Bai, J.; and Chintala, S. 2019. PyTorch: An Imperative Style, High-Performance Deep Learning Library. In Wallach, H. M.; Larochelle, H.; Beygelzimer, A.; d'Alché-Buc, F.; Fox, E. B.; and Garnett, R., eds., *Annual Conference on Neural Information Processing Systems*, 8024–8035.
- Qian, R.; Wei, Y.; Shi, H.; Li, J.; Liu, J.; and Huang, T. 2019. Weakly Supervised Scene Parsing with Point-Based Distance Metric Learning. In *Proceedings of the AAAI Conference on Artificial Intelligence*, 8843–8850.
- Rawat, S. S.; Verma, S. K.; and Kumar, Y. 2020. Review on recent development in infrared small target detection algorithms. *Procedia Computer Science*, 167: 2496–2505.
- Wang, H.; Zhou, L.; and Wang, L. 2019. Miss Detection vs. False Alarm: Adversarial Learning for Small Object Segmentation in Infrared Images. In *Proceedings of the IEEE/CVF International Conference on Computer Vision*, 8508–8517.
- Wei, Y.; Liang, X.; Chen, Y.; Shen, X.; Cheng, M.-M.; Feng, J.; Zhao, Y.; and Yan, S. 2017. STC: A Simple to Complex Framework for Weakly-Supervised Semantic Segmentation. *IEEE Transactions on Pattern Analysis and Machine Intelligence*, 39(11): 2314–2320.
- Wu, P.; Huang, H.; Qian, H.; Su, S.; Sun, B.; and Zuo, Z. 2022. SRCANet: Stacked Residual Coordinate Attention Network for Infrared Ship Detection. *IEEE Transactions on Geoscience and Remote Sensing*, 60: 1–14.
- Yang, B.; Zhang, X.; Zhang, J.; Luo, J.; Zhou, M.; and Pi, Y. 2024. EFLNet: Enhancing Feature Learning Network for Infrared Small Target Detection. *IEEE Transactions on Geoscience and Remote Sensing*, 62: 1–11.
- Ying, X.; Liu, L.; Wang, Y.; Li, R.; Chen, N.; Lin, Z.; Sheng, W.; and Zhou, S. 2023. Mapping degeneration meets label evolution: Learning infrared small target detection with single point supervision. In *Proceedings of the IEEE/CVF Conference on Computer Vision and Pattern Recognition*, 15528–15538.

Yuan, S.; Qin, H.; Yan, X.; Akhtar, N.; and Mian, A. 2024. SCTransNet: Spatial-Channel Cross Transformer Network for Infrared Small Target Detection. *IEEE Transactions on Geoscience and Remote Sensing*, 62: 1–15.

Zhang, J.; and Tao, D. 2021. Empowering Things With Intelligence: A Survey of the Progress, Challenges, and Opportunities in Artificial Intelligence of Things. *IEEE Internet of Things Journal*, 8(10): 7789–7817.

Zhang, M.; Yang, H.; Guo, J.; Li, Y.; Gao, X.; and Zhang, J. 2024. IRPruneDet: Efficient Infrared Small Target Detection via Wavelet Structure-Regularized Soft Channel Pruning. In *Proceedings of the AAAI Conference on Artificial Intelligence*.

Zhang, M.; Yue, K.; Zhang, J.; Li, Y.; and Gao, X. 2022a. Exploring Feature Compensation and Cross-level Correlation for Infrared Small Target Detection. *Proceedings of the 30th ACM International Conference on Multimedia*.

Zhang, M.; Zhang, R.; Yang, Y.; Bai, H.; Zhang, J.; and Guo, J. 2022b. ISNet: Shape matters for infrared small target detection. In *Proceedings of the IEEE/CVF Conference on Computer Vision and Pattern Recognition*, 877–886.